Computational study of tetrahedral Al–Si ordering in muscovite

Article *in* Physics and Chemistry of Minerals · September 2001

DOI: 10.1007/s002690100184

CITATIONS
59

READS
374

6 authors, including:

Martin Travis Dove
Queen Mary, University of London
453 PUBLICATIONS **13,251** CITATIONS

SEE PROFILE

Simon Redfern
Nanyang Technological University
399 PUBLICATIONS **9,249** CITATIONS

SEE PROFILE

Claro Ignacio Sainz-Díaz
Instituto Andaluz de Ciencias de la Tierra
165 PUBLICATIONS **2,833** CITATIONS

SEE PROFILE

Phys Chem Minerals (2001) 28: 534–544

ORIGINAL PAPER

E. J. Palin · M. T. Dove · S. A. T. Redfern
A. Bosenick · C. I. Sainz-Diaz · M. C. Warren

Computational study of tetrahedral Al–Si ordering in muscovite

Received: 28 August 2000 / Accepted: 12 March 2001

Abstract The nature of Al–Si ordering across the tetrahedral sites in muscovite, $K_2Al_4(Si_6Al_2O_{20})(OH)_4$, was investigated using various computational techniques. Values of the atomic exchange interaction parameters J_l were obtained. From these parameters, a two-dimensional Al–Si ordering scheme was deduced. The transition temperature T_c for this two-dimensional ordering is 1900 K. There are several possible ordering schemes in three dimensions, based on different stacking sequences of ordered sheets of tetrahedral sites. Monte Carlo simulations of both two-dimensional and three-dimensional ordering were performed, but in the three-dimensional simulation only the two-dimensional ordering is seen, implying that three-dimensional ordering is too slow to be attained during the timescale of the simulation. The effect of the three-dimensional interactions is to raise the two-dimensional ordering temperature to 2140 K. From the three-dimensional Monte Carlo simulation, the frequency of occurrence of 4Si0Al, 3Si1Al, 2Si2Al and 1Si3Al clusters was determined, which match those inferred by ^{29}Si MAS–NMR measurements reasonably well. In fact, the match suggests that the cation ordering seen in experiments corresponds to a configuration with considerable short-range order but no long-range order, similar to a state that is at a temperature just above an ordering phase transition.

E. J. Palin · M. T. Dove (✉) · S. A. T. Redfern
A. Bosenick · M. C. Warren
Department of Earth Sciences, University of Cambridge,
Downing Street, Cambridge CB2 3EQ, UK
e-mail: martin@esc.cam.ac.uk

C. I. Sainz-Diaz
Estacion Experimental del Zaidin, CSIC,
C/Profesor Albareda, 1, 18008-Granada, Spain

Present addresses:
A. Bosenick
Martenshofweg 9, 24109 Kiel, Germany

M. C. Warren
Department of Earth Sciences,
The University of Manchester, Manchester, M13 9PL

Key words Muscovite · Al–Si ordering · Layer silicates · Phase transitions · Monte Carlo simulations

Introduction

The phenomenon of Al–Si ordering in aluminosilicate minerals has long been recognised as one of the important aspects of mineral behaviour, particularly since it can have a significant effect on thermodynamic properties. Recently, we have used computer simulations to complement experimental data, particularly using a combination of lattice energy methods to calculate ordering energies and Monte Carlo simulations to calculate the dependence of ordering on temperature (Thayaparam et al. 1994, 1996; Dove et al. 1996, 2000; Dove 1999). Among the main findings of these studies were that the exact Al:Si ratio can have a considerable effect on the ordering temperatures (Dove et al. 1996; Myers et al. 1998), particularly as this ratio decreases from 1:1, and that the detailed topology of the structure can provide ways to allow short-range order to develop without necessarily forcing long-range order to be established (Dove et al. 1996), thereby leading to a considerable reduction in the ordering temperature that would be predicted by methods that consider only coordination numbers (such as Bragg–Williams and other lower-order cluster variation methods). Both factors come into play in a significant way in the ordering process in cordierite (Thayaparam et al. 1996). At the simplest level, Al–Si ordering can be said to be driven by the phenomenon of aluminium avoidance (Löwenstein's rule), that is, that in equilibrium there is a driving energy that acts to avoid the formation of Al–O–Al linkages. The effect of a low Al:Si ratio allows the possibility of avoiding formation of any Al–O–Al linkages without the need for long-range ordering. In this case, the driving force for long-range order comes from interactions between tetrahedral sites that are not nearest neighbours (Dove et al. 1996).

In this work we extend the study of Al–Si ordering in minerals to the layer silicate group, specifically to muscovite, $K_2Al_4(Si_6Al_2O_{20})(OH)_4$. Computer modelling is a valuable tool in the case of muscovite and similar hydrated minerals because experimental investigation over a wide range of temperatures is not possible due to the dehydroxylation and breakdown that would occur on heating. A computational study of Al–Si ordering in muscovite is relevant for three other reasons. First, as part of our own ongoing programme of work on modelling cation ordering in minerals, layer silicates are of interest because of the low Al:Si ratio of 1:3 (as compared with 1:2 in leucite, 4:5 in cordierite and 1:1 in anorthite). Second, muscovite is a hydrogen-bearing mineral, and our methods have yet to be extended to systems such as these. Hence part of our objective in this paper is to demonstrate that one can make progress with hydrated minerals. Third, there have been a number of other studies of Al–Si ordering in muscovite and related materials using experimental probes such as NMR (Herrero et al. 1985, 1986, 1987, 1989; Circone et al. 1991), and computational methods based either on lattice energy relaxation methods (Collins and Catlow 1992) or computationally more intensive methods such as Monte Carlo and the cluster variation method, or by simpler statistical methods using simple constraints, electrostatic interactions or inverse methods (Herrero et al. 1985, 1986, 1987, 1989; Circone et al. 1991; Herrero and Sanz 1991; Vinograd and Putnis, 1998). The latter methods gave atomic configurations which were used to predict the NMR spectra for comparison with the experimental data.

The structure of muscovite is shown in Fig. 1. It is comprised of sheets of AlO_6 octahedra, hereafter referred to as octahedral sheets, which are sandwiched between two sheets of AlO_4 and SiO_4 tetrahedra, hereafter referred to as the tetrahedral sheets. The apices of the tetrahedra in the lower sheet point upward, and the apices of the tetrahedra in the upper sheet point downwards. Such a unit of one octahedral sheet and two tetrahedral sheets will hereafter be referred to as a layer. The presence of AlO_4 tetrahedra results in a net negative charge that is compensated by a sheet of K cations between two layers. All sheets are parallel to the (001) planes. The existence of sheets of tetrahedra allows the possibility of two-dimensional ordering within the sheets. Three-dimensional ordering can occur only if there are significant interactions between the sheets, but these interactions will span distances of 5 Å or more. Part of our objective in this study is to consider the relationship between two-dimensional and three-dimensional ordering processes.

In this work we consider the ordering of Al and Si across the tetrahedral sites in muscovite. In other micas the octahedral sheets can contain more than one type of cation, so that ordering across the octahedral sites will also need to be considered. The extension of this study to incorporate ordering in octahedral sheets will be the subject of a future paper.

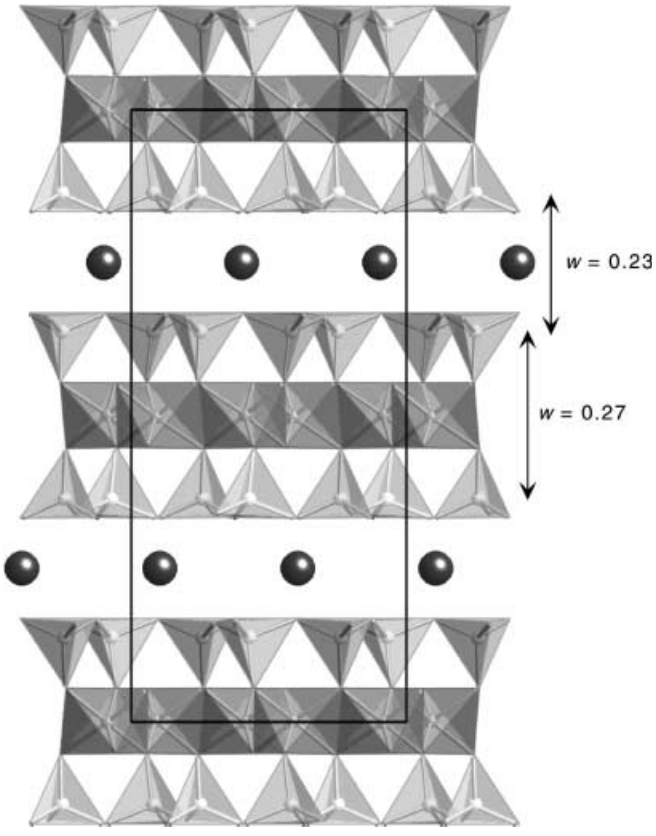

Fig. 1 Crystal structure of muscovite, showing sheets of tetrahedra and octahedra, forming layers. The differences in z coordinates between the tetrahedral sheets, denoted by w, are indicated since these are used to describe the tetrahedral ordering interactions. The unit cell is indicated by the *box*: this includes two layers

Methods

Basic strategy

The approach we take for the simulation of cation ordering processes is to first use empirical interatomic potentials and lattice energy relaxation methods to compute ordering interactions, and then to use Monte Carlo simulations to simulate the ordering process as a function of temperature (Dove 1999; Dove et al. 2000; Bosenick et al. 2001; Warren et al. 2001). The approach makes use of a model Hamiltonian for the ordering interactions, which we refer to as the J formalism. If we assume separate pair interactions for two ordering cations, say Si and Al as in the present study, the energy may be written as:

$$E = E_0 + \sum_n N^n_{\mathrm{Al-Al}} E^n_{\mathrm{Al-Al}} + N^n_{\mathrm{Si-Si}} E^n_{\mathrm{Si-Si}} + N^n_{\mathrm{Si-Al}} E^n_{\mathrm{Si-Al}} \ , \qquad (1)$$

where n indicates different types of neighbouring pairs of cations (for example, pairs with different separations), and the total energy requires summation over all types of interactions. It can be shown that this energy can be reduced to:

$$\begin{aligned} E &= E'_0 + \sum_n N^n_{\mathrm{Al-Al}} \left(E^n_{\mathrm{Al-Al}} + E^n_{\mathrm{Si-Si}} - 2E^n_{\mathrm{Si-Al}} \right) \\ &= E'_0 + \sum_n N^n_{\mathrm{Al-Al}} J_n \ . \end{aligned} \qquad (2)$$

This result follows whether or not there are equal numbers of the two types of cations. The separate energy terms for each neighbour

pair have been combined into a single parameter called the exchange interaction, and labelled J. This parameter represents the energy associated with the exchange of two ions to form Al–O–Al and Si–O–Si linkages instead of two Si–O–Al linkages. Equation (2) will be used for the determination of the values of the exchange interactions J.

To proceed with the statistical analysis of the energies, it is useful to define an ordering variable for each site. It actually does not matter (aside from the definition of the base energy, E_0, and a constant factor) how exactly this variable is defined. We take the definition of the site variable σ such that $\sigma = -1$ if the site is occupied by Al and $\sigma = +1$ if the site is occupied by Si. With this definition, it is possible to write the energy in terms of the following model Hamiltonian:

$$H = E_0 + \frac{1}{4}\sum_{\langle ij \rangle} \sigma_i \sigma_j J_n \quad . \tag{3}$$

The angular brackets below the summation sign indicate that the sum is over all relevant pairs of tetrahedral sites, and avoids counting any pair twice. E_0 is a constant that absorbs all other components of bond energies, and has no effect on the ordering process. The model Hamiltonian holds for all values of the Al:Si ratio, although it usually only derived in textbooks for the special case where the Al:Si ratio is 1:1. A more detailed discussion has been given elsewhere (Bosenick et al. 2001). The model Hamiltonian of Eq. (3) is particularly amenable for analysis by the tools of statistical mechanics such as the Monte Carlo method used in this paper (Warren et al. 2001).

Model interatomic potentials

The task of the first stage in the modelling process is to derive values of the J parameters, which, as mentioned above, is accomplished using empirical model interatomic potentials and lattice energy relaxation methods. A number of previous studies (for example, Post and Burnham 1986; Patel et al. 1991; Winkler et al. 1991; Collins and Catlow 1992; Dove et al. 1993; Thayaparam et al. 1994) have shown that crystal structures can be simulated with reasonable accuracy using model interatomic potentials.

Apart from the hydroxyl ions, all the ions in our model are modelled using formal charges. The O and H ions within the hydroxyl groups are given non-formal charge values, although the overall charge on the hydroxyl molecular ion has a formal charge of $-1e$. Four types of model interatomic potential are necessary to model the short-range interactions in muscovite, which we now describe using the general symbols E to represent energy, r to represent an interatomic distance, θ to represent an angle between two interatomic vectors, and using a zero subscript to indicate an equilibrium value. Short-range Si–O, Al–O, K–O and O–O interactions are modelled by Buckingham energy potentials, of the form

$$E = A\exp(-r/\rho) - Cr^{-6} \quad . \tag{4}$$

For Al–O and K–O potentials the parameter C has zero value. O–Si–O tetrahedral interactions and O–Al–O tetrahedral and octahedral interactions are modelled by three-body potentials, of the form

$$E = \frac{1}{2}k(\theta - \theta_0)^2 \quad . \tag{5}$$

O–H interactions within the hydroxyl molecular ions are modelled by a Morse potential, which has the form

$$E = D\Big[\,(1 - \exp[-a(r - r_0)])^2 - 1\Big] \quad . \tag{6}$$

All the O atoms except those forming part of the hydroxyl ions are modelled by the shell model, in which they are considered to consist of a core comprising the nucleus and tightly bound inner electrons, surrounded by a massless shell of the remaining outer electrons. The cores are assigned a charge of $+0.84819e$ and the shells a charge of $-2.84819e$, maintaining the formal value for the overall ionic charge. The core and shell are held together by a harmonic core–shell interaction, of the form

$$E = \frac{1}{2}Kd^2 \quad , \tag{7}$$

where d is the separation of the centres of the core and shell.

The values of the various coefficients were taken from a number of different sources, which were brought together and tested in detail by Winkler et al. (1991) and Patel et al. (1991). These two studies showed that the models give good results for structures and dynamic properties of a wide range of aluminosilicates. These studies also confirmed that the model is transferable across a wide range of structures, so that it might be used with reasonable confidence on structures not included in the original tests. The models have been tested in more detail for a wide range of layer silicates with different chemical compositions by Sainz-Diaz et al. (2001). Details of the values used for various potentials can be found in Table 1.

The lattice energy minimisation procedure was carried out using the program GULP written by Gale (1997). This is able to handle all the interactions of our model, including the shell model and bond-bending terms. The electrostatic energy is summed using the Ewald method. Full details are given in the reference.

Model testing

Not only has the model been tested for structures as discussed above, it has also been used in previous studies of Al/Si ordering which have shown that it can give reasonable values for the J parameters (Dove et al. 1993; Thayaparam et al. 1994, 1996; Dove et al. 2000). For the present application, we tested the model for its application to muscovite, in particular to test the use of the potentials involving the hydrogen atom, by calculating the equilibrium structure assuming complete cation disorder, and comparing against the experimental structure of Catti et al. (1994). In this structure, the formula unit is $K_2Al_4(Si_6Al_2O_{20})(OH)_4$, space group $C2/c$ (monoclinic), with cell parameters $a = 5.2108$ Å; $b = 9.0399$ Å; $c = 20.021$ Å, $\beta = 95.76°$. The relaxed structure had lattice parameters 5.2104, 9.0568, 19.7104 and 96.121 Å, respectively, which agree with the experimental values to better than 1.5%. The mean tetrahedral cation–O distance was 1.642 Å (experiment) and 1.648 Å (calculation), the mean octahedral Al–O distance was 1.947 Å (experiment) and 1.888 Å (calculation), the mean octahedral Al–OH distance was 1.935 Å (experiment) and 1.933 Å (calculation), the mean K–O distance was 2.896 Å (experiment) and 2.865 Å (calculation), and the mean O–H distance was 0.947 Å (experiment) and 0.979 Å (calculation). Clearly there is good agreement for all distances, the worst being the octahedral Al–O and O–H distances, which have a 3% discrepancy, but the other distances agree to within 1%. This level of agreement is typical of what can be achieved for many aluminosilicates with the same model interatomic potential.

Determination of the exchange interactions in muscovite

Fourteen different exchange interactions, labelled J_1–J_{14}, were assigned according to the shortest different interatomic distances in the crystal. To assist in interpretation, we have assigned a parameter w to represent the difference in z (in fractional coordinates) between any two interacting atoms. This enables the exchange interactions to be grouped, with $w = 0$ indicating interactions between two atoms in the same tetrahedral sheet (i.e. intrasheet), $w = 0.27$ indicating interactions between two atoms in the different tetrahedral sheets in the same layer (intersheet), and $w = 0.23$ indicating interactions between two atoms in tetrahedral sheets in two separate layers (interlayer). These groups are illustrated in Fig. 1. The distances associated with the 14 exchange interactions are shown in Table 2. Examples of the distances corresponding to the exchange interactions for $w = 0$ are shown in Fig. 2.

Table 1 Values used in the model interatomic potentials for muscovite. The interaction types are defined by Eq. (4) Buckingham, (6) Morse, (7) spring (core–shell), (5) three-body

Potential type	Atoms	Parameter values				
		A (eV)	ρ (Å)	C (eV · Å^6)	r_{max} (Å)	
Buckingham	Si core–O1 core	999.9	0.3012	0	8	
Buckingham	Si core–O2 shell	1283.9077	0.3205	10.66	8	
Buckingham	Al core–O1 core	1142.6772	0.29912	0	8	
Buckingham	Al core–O2 shell	1460.3	0.29912	0	8	
Buckingham	K core–O shell	65269.7	0.213	0	8	
Buckingham	O shell–O shell	22764	0.149	27.88	8	
Buckingham	H core–O2 shell	325	0.25	0	8	
		D (eV)	a (Å^{-1})	r_0 (Å)	r_{max} (Å)	
Morse	O1 core–H core	7.0525	2.1986	0.9485	1.4	
		K (eV · Å^{-2})				
Spring (core–shell)	O core–O shell	74.92				
		k (eV rad^{-2})	θ_0 (°)	r_{max} (Å) (1–2)	r_{max} (Å) (2–3)	r_{max} (Å) (1–3)
Three-body	O shell–Al1 core–O shell	2.0974	109.47	1.8	1.8	3.2
Three-body	O shell–Si core–O shell	2.0974	109.47	1.8	1.8	3.2
Three-body	O shell–Al2 core–O shell	2.0974	90	2.2	2.2	3.2

The procedure used to derive values of the J parameters is to use a supercell with periodic boundary conditions, and to calculate the energy for many configurations, with the ordering cations in different positions in each configuration. The supercell was constructed as a $2 \times 1 \times 1$ multiple of the C-centred monoclinic unit cell. The supercell contained 32 tetrahedral sites.

Fifty configurations were generated using the spreadsheet methods described by Bosenick et al. (2001), placing 8 Al and 24 Si cations on the tetrahedral sites. The spreadsheet method was modified by imposing the constraint that the electrostatic charge balance is preserved in each layer within the cell. Each of these 50 configurations was optimised using the GULP lattice energy minimisation program. Previous experience had shown that allowing relaxation of the volume makes no difference to the final analysis. The lattice parameters were fixed at values obtained by an energy minimisation calculation run with each tetrahedral site having partial occupancies of Si and Al atoms corresponding to complete disorder. The energy minimisation of the different configurations provided 50 different lattice energies, which formed a set of values for E in Eq. (2).

The spreadsheet analysis generated the number of Al–Al interactions of each exchange pair for each configuration, so that, coupled with the energy, the procedure gave 50 equations of the form of Eq. (2) with the values of the exchange interactions to be determined by linear regression. The values for E_0 and all 14 Js are given in Table 2. The relative statistical significance of each of the fitted values is given in the output from the linear regression, and to simplify subsequent calculations the statistically insignificant values and the values that were close to zero were then artificially set to zero. The effect on the overall fit of the calculated energies was found to be negligible. It should be noted that there are correlations between some of the values of the exchange constants. These give rise to the relatively large errors shown in Table 2. Because of the correlations, the errors do not imply that the values are statistically insignificant. Instead, they imply that if any of the parameters are removed there will be correlated changes to the other parameters required. The quality of the agreement between the values of the lattice energies of the different configurations and the corresponding values of the model Hamiltonian is shown in Fig. 3.

The values of the exchange constants given in Table 2 are comparable to the Al/Si exchange constants obtained for other aluminosilicates (e.g. Thayaparam et al. 1994, 1996; Dove et al. 2000). The value of J_1 is within the range of other materials, although on the large side of this range. The values for the more distant neighbour exchange constants are similar to those obtained for other systems.

Table 2 Assigned J parameters. The parameters for which a range of values is shown were deemed to be sufficiently similar to group them together, e.g. for J_1, the distance ranged from 2.97 to 3.08 Å, but the type of interaction (nearest-neighbour) was the same. The fitted values marked with an *asterisk* were set to zero in the subsequent Monte Carlo simulations. Errors on the fitted values, given in *brackets* as the error on the last figure, are those given by the fitting routine. Some errors appear rather large because of correlations in the fitting procedure

Interaction	w	Distance (Å)	Fitted value (eV)
J_1	0	2.97–3.08	1.0(1)
J_2	0	5.22	0.23(5)
J_3	0	5.96–6.05	0.00(5)*
J_4	0	7.92–8.04	0.13(4)
J_5	0.27	5.56	0.38(14)
J_6	0.27	5.69	−0.07(10)*
J_7	0.27	6.24	−0.05(12)*
J_8	0.27	6.47	0.11(13)
J_9	0.27	6.96	0.15(13)
J_{10}	0.27	7.02	0.07(9)
J_{11}	0.23	4.51	0.0(2)*
J_{12}	0.23	5.41–5.46	−0.16(16)
J_{13}	0.23	6.82–6.98	−0.1(1)
J_{14}	0.23	7.48–7.55	−0.08(9)

Monte Carlo methods

We remarked above that the Monte Carlo (MC) method is suitable for statistical analysis of the Hamiltonian of Eq. (3). In application to cation ordering studies, the σ variables of two sites are exchanged in each update step. For this work we used our own program, Ossia98 (Warren et al. 2001). This has been written for use on large parallel computers, with the intention of performing parallel simulations of many different temperatures. Further details of Ossia98 are found on the *www* at http://www.esc.cam.ac.uk/ossia/.

The output of the MC runs includes a number of expectation values, including $\langle E \rangle$ and $\langle E^2 \rangle$ for the energy, and $\langle Q \rangle$ and $\langle Q^2 \rangle$ for the order parameter (defined below). From these expectation values it is possible to form the heat capacity C and susceptibility χ.

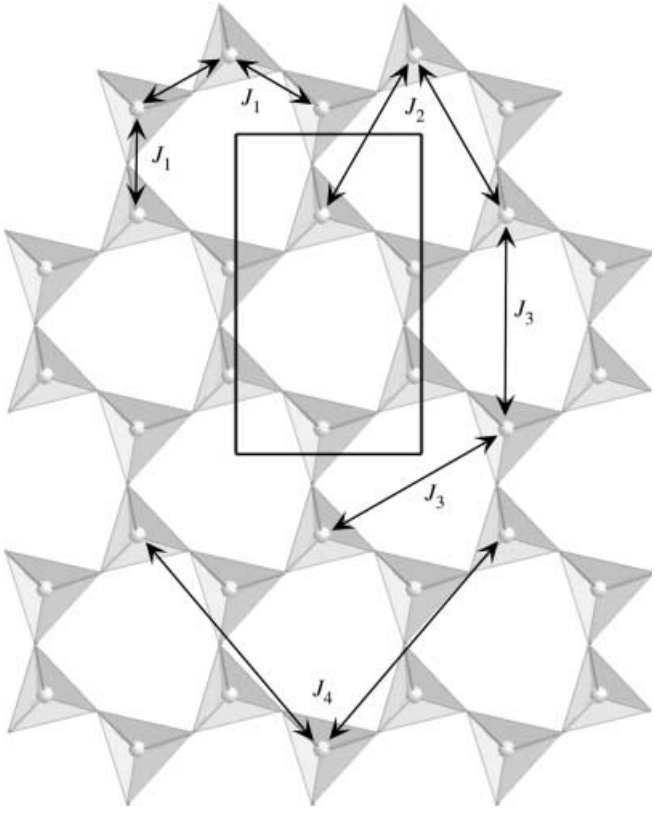

Fig. 2 The four important exchange interactions within a single ($w = 0$) tetrahedral sheet. The rectangular box indicates one unit cell

$$C = \frac{\langle E^2 \rangle - \langle E \rangle^2}{k_B T^2} \tag{8}$$

$$\chi = \frac{\langle Q^2 \rangle - \langle Q \rangle^2}{k_B T} \quad . \tag{9}$$

In the study of phase transitions, these quantities are useful as independent measurements of the ordering temperature T_c. This can be determined as the temperature at which the order parameter falls to zero, but at temperatures close to T_c there are large fluctuations in Q and the actual value of T_c can be difficult to determine. At a second-order phase transition, the values of both C and χ will diverge at T_c, and the temperatures at which these two quantities diverge provide two additional estimates of the value of T_c.

Ossia98 has also been programmed to calculate cluster probabilities. Specifically, in this work we calculated the probabilities of forming clusters of four cations with a central Si and three cations in the surrounding triangle in the sheets of the muscovite structure. These clusters are what are measured in ^{29}Si magic-angle spinning NMR experiments, so there is a direct point of contact between the MC simulations and experimental data. These clusters are shown in Fig. 4 for future reference. The figure also gives the probability of each cluster if there is completely random distribution of the Si and Al cations. In the fully ordered state given by our model (see below), the probability of the cluster linking one Si cation to two other Si cations and one Al cation is equal to 1, and the other cluster probabilities equal zero.

The configurations produced by the MC simulation were inspected using the Cerius^2 crystal-drawing program. This enabled the identification of ordered structures, and, in particular, identified cases where ordering was accompanied by the formation of domain microstructures.

The order parameter for a cation ordering phase transition can be defined in terms of the relative proportions of different cations

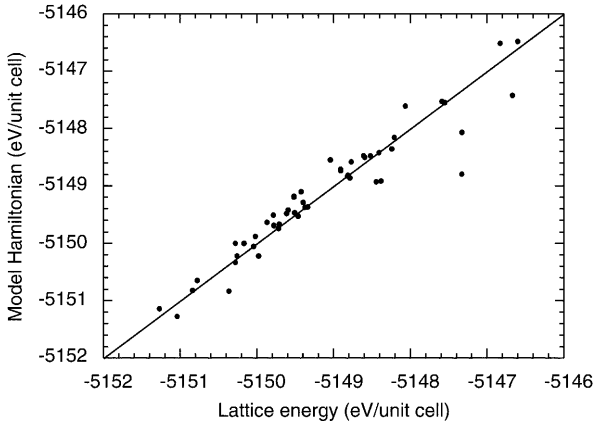

Fig. 3 Comparison of lattice energies of 50 configurations with different Al/Si arrangements calculated using GULP with the corresponding values of the fitted Hamiltonian. The *straight line* corresponds to perfect agreement

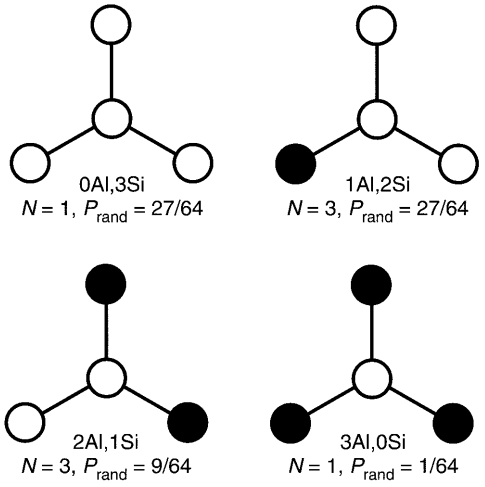

Fig. 4 The four basic clusters of the three tetrahedral sites connected to a silicon tetrahedral site in a sheet of tetrahedra in muscovite. The *filled circles* represent the sites occupied by Al, and the *open circles* represent the sites occupied by Si. Against each cluster is given the number of permutations of the cluster, and the probability of finding this type of cluster if the occupancy of the tetrahedral sites is completely random

on specific sites. In the case of Al/Si ordering, we define P_{Al} as the probability of occupancy by Al of a particular type of site that becomes occupied by Al in the ordered phase. In the case of muscovite, the value of P_{Al} will vary between 1/4 and 1 between the fully random and fully ordered states, respectively. Therefore, we can write the order parameter as

$$Q = \frac{4}{3}\left(P_{Al} - \frac{1}{4}\right) \quad , \tag{10}$$

such that the value of Q varies between 0 and 1 between the fully random and fully ordered states, respectively. Similarly, order parameters can be defined for other types of site, in which case the value of P_{Al} will vary between 1/4 and 0, and the prefactor in Eq. (10) will have value of -4 rather than 4/3. The values of the different order parameters for one type of ordering should be equal to each other at all temperatures because the values of P_{Al} for the different types of sites will be correlated. If there are different

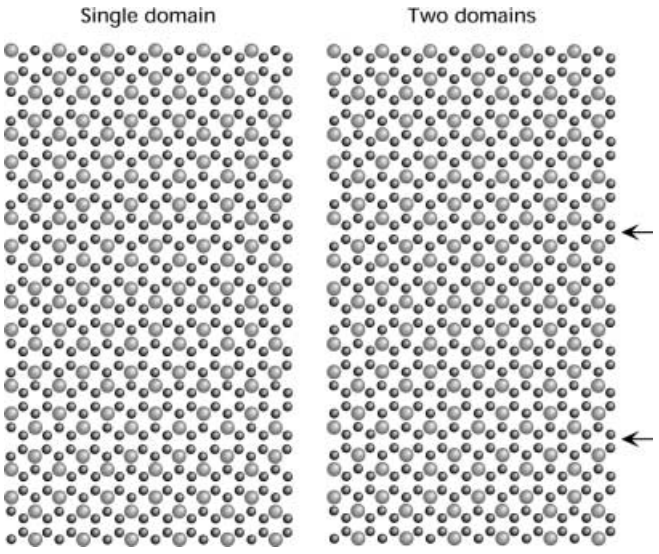

Fig. 5 *Left* Proposed ordered structure based on the relative values of the exchange interactions J_1 to J_4, as confirmed by the Monte Carlo simulations. *Right* Ordered structure containing two domain walls, lying in the horizontal plane, obtained in one run of the Monte Carlo simulations. *Large spheres* represent Al and *small spheres* represent Si

ordering schemes, there will need to be separate sets of definitions of the order parameter for each separate ordering scheme.

Results

Implications of the values of the exchange interactions for two-dimensional and three-dimensional ordering

The relevant exchange interactions for two-dimensional ordering, that is, the ordering in one tetrahedral sheet, are J_1–J_4 in Table 2. Since $J_3 \approx 0$, and J_1 and J_2 are both positive, an ordered tetrahedral sheet is most likely to have Al atoms in J_3 positions, as illustrated in Fig. 5, in order to avoid forming Al–Al linkages in the J_1 and J_2 positions. Whilst this gives ordering within a single hexagon, there are several ways in which this ordering can span the whole sheet. The different possibilities are differentiated by the positive J_4 interaction. As a result, the only ordering pattern that avoids formation of Al–Al interactions in the J_4 positions is that shown in Fig. 5.

It is less clear what happens in the case of three-dimensional ordering. We make the reasonable assumption, based on the relative sizes of the exchange interactions, that a three-dimensional ordered structure is a combination of the two-dimensional ordered sheets discussed above, with a particular stacking sequence that is determined by the intersheet and interlayer exchange interactions. There are eight possible configurations for stacking of the ordered sheets, which are shown in Fig. 6 and labelled A–H. These are in two groups, since alternate sheets have the tetrahedral sites offset with respect to each other.

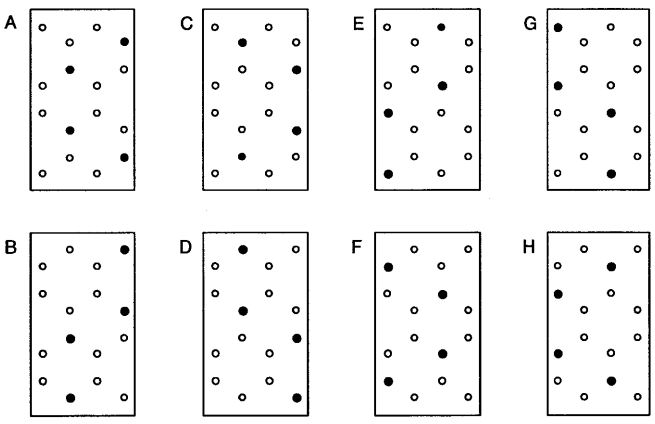

Fig. 6 Eight possible configurations for stacking of the ordered sheets. The *top four* (A, C, E, G) correspond to one sheet in a layer, and the *lower four* (B, D, F, H) to the other sheet in the same layer

To investigate further the three-dimensional ordering, the lowermost tetrahedral sheet in the unit cell (at $z = 0.13$) was constrained to be of configuration C (the choice is arbitrary with the form of the model Hamiltonian). There are therefore $4^3 = 64$ possible combinations of four sheets in the unit cell. The $N_I J_I$ values for each of these combinations were calculated, with the lowest value of $N_I J_I$ giving the most favourable structure (see Eq. 3). There are of course other possible combinations of sheets (i.e. those in which the $z = 0.13$ sheet is A, E or G) but these are actually the same structures with the unit-cell origin shifted.

The $N_I J_I$ values were verified by performing complete energy minimisations of the structures with different sheet combinations. The comparison of the $N_I J_I$ values with the corresponding lattice energies is shown in Fig. 7. There is good agreement between the two sets of energies, allowing for the approximations inherent in the use of the model Hamiltonian, and it is clear that the same structure has the lowest energy in both cases. In addition, almost all points on the figure correspond to degenerate structures and, more importantly, there are degenerate lowest energy structures.

Monte Carlo simulations of two-dimensional ordering

The two-dimensional ordered structure proposed by consideration of the exchange interactions J_1 to J_4 discussed above was confirmed by performing Monte Carlo simulations using a sample containing only a single sheet of tetrahedral sites; that is, one tetrahedral sheet from a $12 \times 12 \times 1$ supercell of muscovite. Simulations were performed starting from initial configurations that were both ordered and disordered for a wide range of temperatures. The simulations confirmed that the ordered structure shown in Fig. 5 is the true ordered structure. In some cases, the ordered structure was produced with domain walls; an example is shown in Fig. 5 alongside the perfect ordered structure.

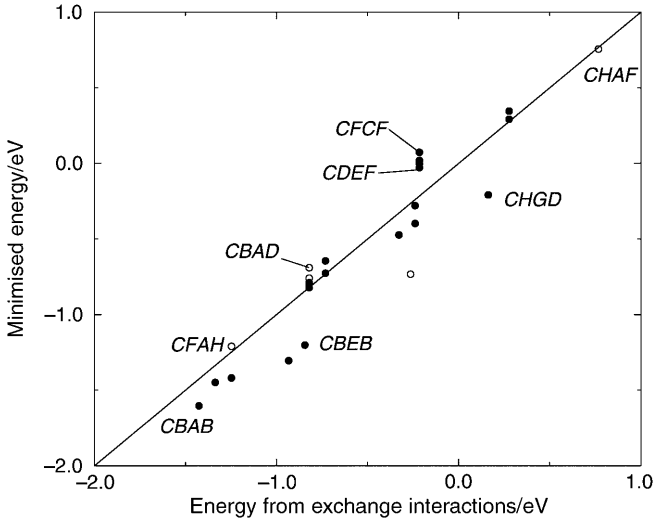

Fig. 7 Correlation between the values of the energy of the different possible three-dimensional ordered structures calculated from the exchange interactions and the corresponding energies calculated by energy minimisation. The *zero point* on the axes corresponds to the energy E_0 of the model Hamiltonian, and the *line* indicates perfect agreement. A number of tetrahedral sheet combinations are annotated by way of example; the sheet configurations A–H are given in Fig. 6. Points corresponding to degenerate structures are denoted by *closed circle* symbols; those representing single structures are denoted by *open circles*

The temperature dependence of the order parameter, heat capacity and susceptibility are shown in Fig. 8. From these plots is can be seen that the order–disorder transition occurs at a temperature of 1900 K. For two-dimensional ordering, we expect the standard Ising-model result to hold:

$$Q \propto (T_c - T)^{1/8} \quad . \tag{11}$$

The order-parameter data of Fig. 8 are consistent with this Ising-model behaviour at temperatures close to T_c. The susceptibility curves also scale according to the two-dimensional Ising-model result, namely as

$$\chi^{-1} \propto |T_c - T|^{7/4} \quad . \tag{12}$$

The cluster probabilities defined earlier were calculated as a function of temperature, and are plotted in Fig. 9. It can be seen that there is a considerable degree of short-range order over a range of temperatures above T_c. In fact, the variation towards completely random disorder on heating is remarkably slow, as will be discussed below with regard to the simulations with the three-dimensional ordering.

Results for three-dimensional ordering

The MC simulations of the three-dimensional samples were performed with a $12 \times 12 \times 6$ supercell of the muscovite unit cell with all exchange interactions included. However, these simulations proved to be very difficult. It appeared that the two-dimensional ordering process sets in first on cooling, but the behaviour of the simulations on further cooling was inconsistent. No three-dimensional long-range order was produced. This is straightforward to understand. Since the relative values of the intrasheet exchange interactions are rather larger than those of the intersheet and interlayer exchange interactions, it is not surprising that the ordering within the sheets occurs first on cooling. However, the ordering within each sheet will be almost independent of the ordering within neighbouring sheets. Therefore, when the sample is cooled to a temperature at which three-dimensional ordering should occur, there are now kinetic constraints associated with the need to completely rearrange the ordering in the sheets in order to align the cation distributions within neighbouring sheets. The kinetics are far too slow for equilibrium ordering to be achieved within the constraints of the MC simulations. As a result, it proved to be impossible to simulate the three-dimensional order process when cooling a sample that was set up with a completely random initial configuration of cations.

In order to examine the ordering phase transition in the three-dimensional sample, we ran the MC simulations starting from a fully ordered three-dimensional arrangement of cations, monitoring the changes in ordering on heating. In Fig. 8 we plot the temperature dependence of the two-dimensional order parameter together with the heat capacity and susceptibility in the three-dimensional sample. These have forms similar to those in the two-dimensional simulation (also in Fig. 8), except that the ordering temperature in the three-dimensional simulation, 2140 K, is slightly higher than in the two-dimensional simulation, and the changes at the phase transition are more rapid in the three-dimensional simulation. No other transition process was observed. It appeared that in the heating runs the kinetic constraints that prevented the formation of long-range three-dimensional order in the cooling runs now work in reverse. When the system wants to disorder, there will still be a high degree of order within the individual sheets, and it is not possible for the sheets to reorder to remove the correlation between the ordering of neighbouring sheets. In consequence, the heating runs produced the temperature dependence for the order parameter that reflects the behaviour in two dimensions, as shown in Fig. 8.

The probabilities of the sheet clusters as a function of temperature in the three-dimensional simulations are compared with the corresponding clusters from the two-dimensional simulations in Fig. 9. Apart from the difference in transition temperature, and the differences in the rates of change around T_c, the cluster data are very similar in the two types of simulations. For this system simulations were performed to very high temperature to monitor the evolution of the cluster probabilities towards the purely random values as given in Fig. 4. It can be seen that at temperatures that are as high as ten times T_c the cluster probabilities depart significantly from the random probabilities. The cluster probabilities quickly change towards

the values of the fully ordered structure on cooling below T_c. We discuss the comparison with experimental data in the next section, because it provides particular information about the ordering in experimental samples.

Discussion

High transition temperature

One of the results from this work that is important to note is that the two-dimensional ordering temperature is higher than one might have expected. The application of the Bragg–Williams model using the exchange interactions J_1 to J_4 gives a calculated value of $T_c = 3790$ K, which is about twice the value found in the MC simulations. It was established many years ago that the Bragg–Williams model overestimates the value of T_c, mostly because of the neglect of the effects of short-range order. Our point of comparison is therefore not with the Bragg–Williams estimate per se, but with the value lowered by a factor to account for the usual effects of short-range order. This factor is taken from Ising-model studies of different lattices with equal numbers of ordering cations. For the honeycomb lattice, this factor is 0.506 (Ashcroft and Mermin 1976), and the transition temperature from the MC simulation is close to the Bragg–Williams estimate corrected by this factor. However, for many systems that have been studied using the approach of this paper, the transition temperature is significantly below the corrected Bragg–Williams value. One of the reasons for this is that the correction factor is obtained for the case of equal numbers of the two types of ordering cations, and the effect of changing the ratio is to cause a dramatic lowering of the transition temperature. This has been documented in detail for Al/Si ordering in framework structures. In the case of muscovite the Al:Si ratio is 1:3, which in some cases is small enough to cause a dramatic lowering of the transition temperature below the Bragg–Williams estimate. However, opposing this trend is the fact that the model in this study has interactions to fourth neighbour, and it is known that distant interactions will raise the transition temperature towards the Bragg–Williams estimate. The results for muscovite show this effect.

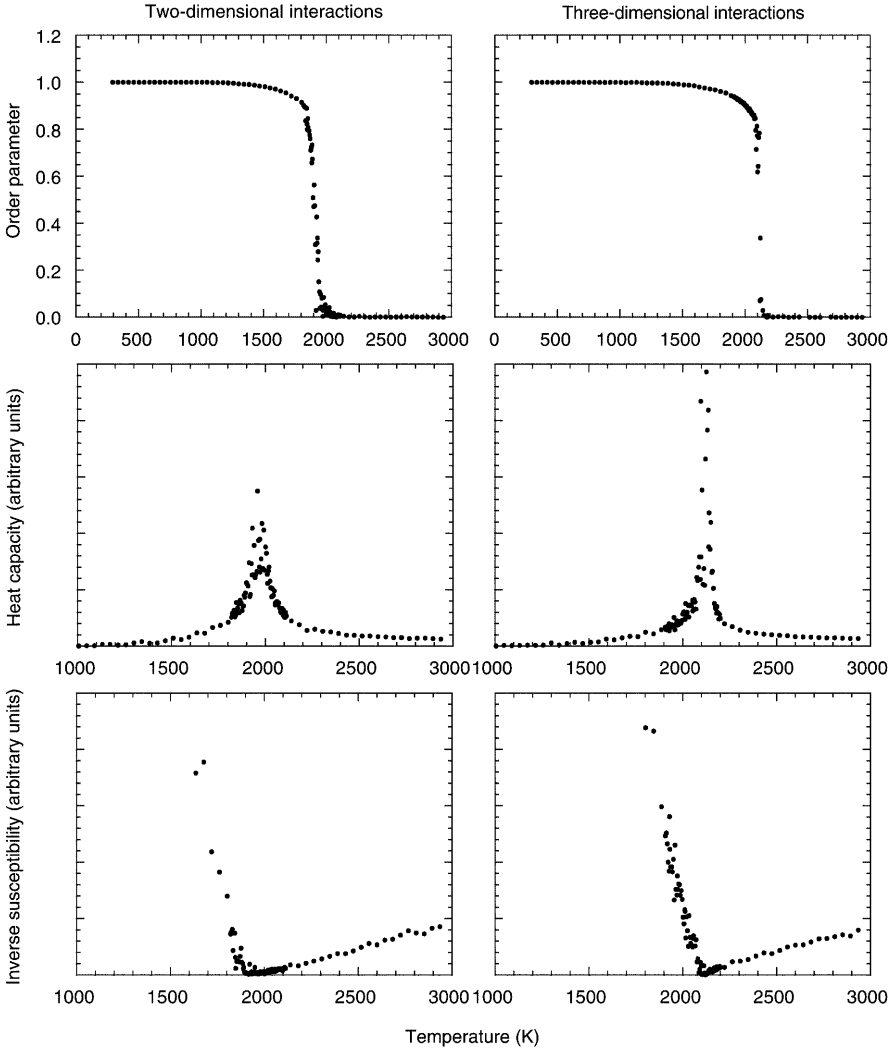

Fig. 8 MC results for the temperature dependence of the order parameter Q, heat capacity and inverse susceptibility χ^{-1}, for simulations with two-dimensional interactions (J_1–J_4) only (*left*) and with all three-dimensional interactions (*right*)

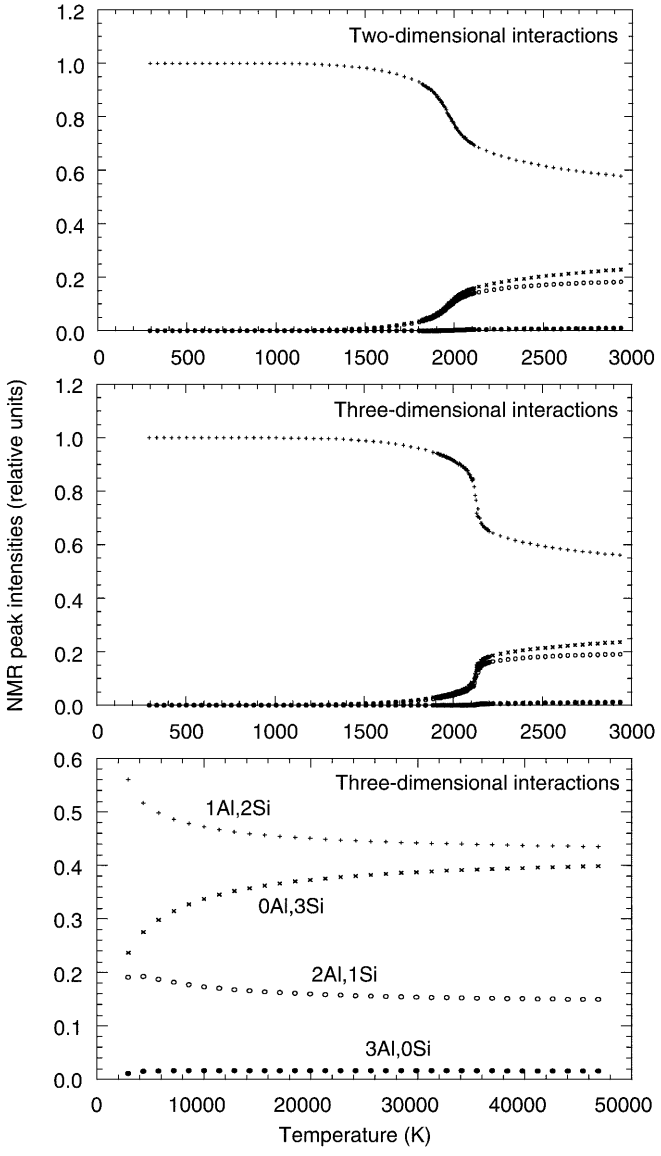

Fig. 9 Temperature dependence of cluster probabilities obtained from the simulations with two-dimensional interactions (*top*) and three-dimensional interactions (*middle*). The *bottom* plot shows the extension of the data for the three-dimensional interactions to very high temperatures. The symbols are *diagonal crosses* for 0Al3Si, *vertical crosses* for 1Al2Si, *open circles* for 2Al1Si, *closed circles* for 3Al0Si, as defined in the bottom plot

Simulation of ^{29}Si MAS–NMR peak intensities

In ^{29}Si MAS–NMR, the peak intensities are proportional to the number of Si atoms in a particular environment in the structure (i.e. Si surrounded by three other Si, by two Si and one Al, etc). Thus, the cluster probabilities given by the MC simulations are directly analogous to the intensity of the normalised peaks in an ^{29}Si MAS–NMR spectrum. A number of ^{29}Si MAS–NMR experimental studies have been performed on layer silicates, including muscovite. These include two series of measurements compiled by Herrero et al. (1987), and one series obtained by Circone et al. (1991), all of which have compositions in the tetrahedral sheets of Al_xSi_{1-x}. Circone et al. (1991) have only one measurement at a value of x close to 0.25, the value in our simulations (note that Circone et al. use a different definition of x, with their value of 0.0 corresponding to our value of 0.25), but Herrero et al. (1987) have several measurements for x between 0.2 and 0.28. The NMR intensities for the relevant set of samples from Herrero et al. (1987) are plotted in Fig. 10. It can be seen that the intensities of the 0Al and 2Al peaks are very sensitive to the exact value of x. In comparison, the intensities of the peaks for the 1Al peak is relatively constant over this range of x. A more detailed analysis of the NMR peak intensities over the whole range of values of x has been given by Herrero et al. (1989) and Circone et al. (1991).

To compare the experimental data with the cluster results of Fig. 9, we start by considering the values of the 1Al2Si clusters, which are the least sensitive to the specific Al content but the most sensitive to temperature. There is a match between the simulation and experimental values (0.577, taken from Fig. 10) at the simulation temperature of 2650 K in the three-dimensional simulation, and at the simulation temperature of 2950 K in the two-dimensional simulation. By matching the values of the 0Al3Si and 2Al1Si cluster probabilities with the NMR data of Fig. 10, it is found that in both cases the best match is for a fractional content of Al of $x = 0.243$ (experimental values from Fig. 10 of 0.23 and 0.19, respectively). This is close enough to the simulation value of $x = 0.25$ to be able to conclude that there is an excellent match between the simulation results and experiment, particularly when it is noted that there is a certain level of uncertainty in the NMR intensities and the actual sample composition. The experimental data of Circone et al. (1991) for the three NMR peak intensities correspond to the simulation temperature of 2859 K in the three-dimensional simulation and the simulation temperature of 3000 K in the two-dimensional simulation. In these simulations the 0Al3Si and 2Al1Si peak intensities correspond to slightly higher temperatures in the simulations, but this could be due to a very slight variation in the chemical composition in the experimental samples as found for the Herrero data.

It is very encouraging that it is possible to map the experimental NMR data and the simulation cluster probabilities as closely as this. The simulations appear to have captured an ordering process that is picked up in the NMR experiments for a range of samples. In so doing, they provide a comment on the ordering in the experimental samples. The discussion above points out that the cation order in the experimental samples corresponds to what would be produced in equilibrium at a temperature above the temperature at which long-range two-dimensional order in the sheets is established. Since the experiments were performed at ambient temperature, it suggests that the cation distribution in the experimental samples has not managed to reach equilibrium on cooling, but that it has passed along a kinetic pathway that goes through the same short-range order states that

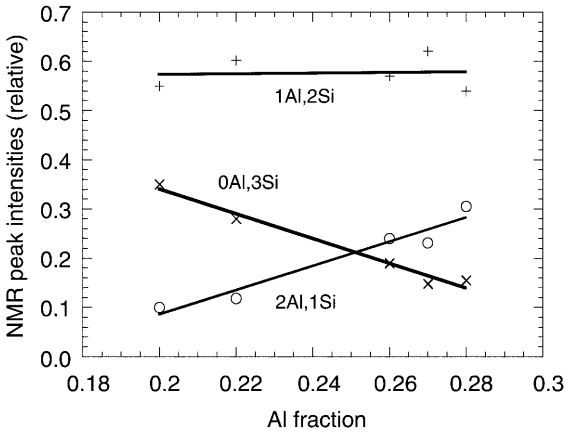

Fig. 10 Dependence of NMR intensities on x in the samples investigated or reported by Herrero et al. (1986). The symbols are *diagonal crosses* for 0Al3Si, *vertical crosses* for 1Al2Si, *open circles* for 2Al1Si, as defined in the plot

would have been achieved at temperatures above an ordering phase transition. The formations of natural or synthetic samples of muscovite are likely to have occurred at temperatures that are much lower than the apparent experimental Al/Si ordering transition temperature. Thus, the first-formed muscovite appears to have no long-range Al/Si order, presumably because of kinetic constraints, and the short-range order that has been observed corresponds to that of a higher temperature.

We are now able to give an interpretation of the cation ordering and the NMR data, building upon the earlier discussion of Herrero et al. (1989). These authors noted that the NMR data are consistent with Löwenstein's law, but the data suggest that there is not perfect long-range order. Herrero et al. (1989) offer a suggestion for the two-dimensional long-range order in the tetrahedral sheets that differs from the one obtained in our MC simulations (Fig. 5). The two structures would actually give similar predictions for the NMR data. The difference arises from the positive value of J_4. The simulation structure is the only structure that avoids forming Al–Al pairs in the J_4 positions, whereas such pairs exist in the Herrero ordered structure. In fact, there are several structures that avoid forming J_1 and J_2 interactions. The Herrero ordered structure allows the formation of J_3 interactions, which is consistent with the calculation of a near-zero exchange constant for this interaction. Even when the number of J_3 interactions is maximised, there are a number of possible ordered structures, which are differentiated on the basis of the strength and sign of the J_4 interactions. The MC simulations have given an understanding of how the degree of order varies with temperature. Herrero et al. (1989) offered a few ideas as to why the NMR data do not show complete long-range order, but they were not in a position to provide an interpretation in terms of an ordering phase transition. By using an inverse simulation it was possible to generate configurations that were consistent with the NMR data. It is now clear from the MC results that there is an ordering phase transition, and that the absence of long-range order in the experimental samples is consistent with the degree of order corresponding to that above the transition temperature.

In a subsequent paper, Herrero and Sanz (1991) obtained an estimate for the value for J_2 of $1.3(2)\mathrm{R}T_{\mathrm{eq}}$, where T_{eq} is the equilibration temperature. Assuming a value for T_{eq} of 2650 K from the above discussion, we calculate $J_2 = 0.30 \pm 0.05$ eV from this estimate. This is in reasonable agreement with the value 0.23 ± 0.05 eV obtained in the present study (Table 2). The agreement is perhaps not surprising, given that the equilibration temperature was located by comparing the MC results with the experimental NMR data, but it does provide a good consistency check of our work and of the methods of Herrero and Sanz (1991).

Acknowledgements We are grateful to NERC, the EU, Acciones Integradas and the Royal Society for financial support. The Monte Carlo simulations were performed on the Hitachi SR2201 parallel computer of the Cambridge High Performance Computing Facility.

References

Ashcroft NW, Mermin ND (1976) Solid state physics. Saunders College Publishing, Fort Worth

Bosenick A, Dove MT, Myers ER, Palin EJ, Sainz-Diaz CI, Guiton B, Warren MC, Craig MS, Redfern SAT (2001) Computational methods for the study of energies of cation distributions: applications to cation-ordering phase transitions and solid solutions. Mineral Mag 65: 193–219

Catti M, Ferraris G, Hull S, Pavese A (1994) Powder diffraction study of $2M_1$ muscovite at room pressure and at 2 GPa. Eur J Mineral 6: 171–178

Circone S, Navrotsky A, Kirkpatrick RJ, Graham CM (1991) Substitution of $^{[6,4]}$Al in phlogopite: mica characterization, unit-cell variation, ^{27}Al and ^{29}Si MAS–NMR spectroscopy, and Al–Si distribution in the tetrahedral sheet. Am Mineral 76: 1485–1501

Collins DR, Catlow CRA (1992) Computer simulation study of structures and cohesive properties of micas. Am Mineral 77: 1172–1181

Dove MT (1999) Order/disorder phenomena in minerals: ordering phase transitions and solid solutions. In: Catlow CRA, Wright K (eds) Microscopic processes in minerals pp 451–475. Kluwer, Amsterdam

Dove MT, Cool T, Palmer DC, Putnis A, Salje EKH, Winkler B (1993) On the role of Al–Si ordering in the cubic-tetragonal phase transition of leucite. Am Mineral 78: 486–492

Dove MT, Thayaparam S, Heine V, Hammonds K (1996) The phenomenon of low Al/Si ordering temperatures in aluminosilicate framework structures. Am Mineral 81: 349–362

Dove MT, Bosenick A, Myers ER, Warren MC, Redfern SAT (2000) Modelling in relation to cation ordering. Phase transitions 71: 205–226

Gale JD (1997) GULP: a computer program for the symmetry-adapted simulation of solids. J Chem Soc Faraday Trans 93: 629–637

Herrero CP, Sanz J (1991) Short-range order of the Si, Al distribution in layer silicates. J Phys Chem Solids 52: 1129–1135

Herrero CP, Sanz J, Serratosa JM (1985) Tetrahedral cation ordering in layer silicates by ^{29}Si NMR spectroscopy. Solid State Comm 53: 151–154

Herrero CP, Sanz J, Serratosa JM (1986) The electrostatic energy of micas as a function of Si, Al tetrahedral ordering. J Phys Cond Matt 19: 4169–4181

Herrero CP, Gregorkiewitz M, Sanz J, Serratosa JM (1987) Si-29 MAS–NMR spectroscopy of mica-type silicates – observed and predicted distribution of tetrahedral Al–Si. Phys Chem Miner 15: 84–90

Herrero CP, Sanz J, Serratosa JM (1989) Dispersion of charge deficits in the tetrahedral sheet of phyllosilicates. Analysis from ^{29}Si NMR spectra. J Phys Chem 93: 4311–4315

Myers ER, Heine V, Dove MT (1998) Thermodynamics of Al/Al avoidance in the ordering of Al/Si tetrahedral framework structures. Phys Chem Miner 25: 457–464

Patel A, Price GD, Mendelssohn MJ (1991) A computer-simulation approach to modeling the structure, thermodynamics and oxygen isotope equilibria of silicates. Phys Chem Miner 17: 690–699

Post JE, Burnham CW (1986) Ionic modeling of mineral structures and energies in the electron gas approximation: TiO_2 polymorphs, quartz, forsterite, diopside. Am Mineral 71: 142–150

Sainz-Diaz CI, Hernandez-Laguna A, Dove MT (2001) Modelling of dioctahedral 2:1 phyllosilicates by means of transferable empirical potentials. Phys Chem Miner 28: 130–141

Thayaparam S, Dove MT, Heine V (1994) A computer simulation study of Al/Si ordering in gehlenite and the paradox of the low transition temperature. Phys Chem Miner 21: 110–116

Thayaparam S, Heine V, Dove MT, Hammonds KD (1996) A computational study of Al/Si ordering in cordierite. Phys Chem Miner 23: 127–139

Vinograd VL, Putnis A (1998) Calculation of the configurational entropy of Al,Si in layer silicates using the cluster variation method. Phys Chem Miner 26: 135–148

Warren MC, Dove MT, Myers ER, Bosenick A, Palin EJ, Sainz-Diaz CI, Guiton B, Redfern SAT (2001) Monte Carlo methods for the study of cation ordering in minerals. Mineral Mag 65: 221–248

Winkler B, Dove MT, Leslie M (1991) Static lattice energy minimization and lattice dynamics calculations on aluminosilicate minerals. Am Mineral 76: 313–331